Ind. J. Pharm. Edu. Res., 10.5530/ijper.20270127.
https://www.ijper.org

Original Article

Conessine Induces Apoptosis Associated with Oxidative Stress and DNA Damage in HCT116 Colorectal Cancer Cells: An *in vitro* and *in silico* Study

Hafiz Antar Makeen[1], Mohammed Albratty[2], Maryam Ahmed Halawi[1,*]

[1]Pharmacy Practice Research Unit, Department of Pharmacy Practice, College of Pharmacy, Jazan University, Jazan, SAUDI ARABIA.
[2]Department of Pharmaceutical Chemistry and Pharmacognosy, College of Pharmacy, Jazan University, Jazan, SAUDI ARABIA.

ABSTRACT

Background: Colorectal Cancer (CRC) is a major health challenge worldwide, prompting the development of effective and safer therapeutic agents. Conessine, a plant-based steroidal alkaloid, exhibits diverse pharmacological benefits; however, its anticancer efficacy and underlying mechanisms in CRC remain underexplored. **Objectives:** The present study intended to investigate the cytotoxicity and apoptosis induced by conessine on HCT116 human CRC cells to elucidate its potential molecular interactions with key apoptotic regulatory proteins. **Materials and Methods:** The cytotoxic effect of conessine was determined using the 3-(4,5-dimethylthiazol-2-yl)-2,5-Diphenyl Tetrazolium Bromide (MTT) assay. Apoptosis and associated morphological changes were quantitatively and qualitatively assessed using Annexin V/PI staining, flow cytometry, and fluorescence-based dual staining (AO/EB). A comet assay was performed to assess the efficacy of conessine in inducing DNA fragmentation. Intracellular ROS levels were assessed using the 2′,7′-Dichlorodihydrofluorescein Diacetate (DCFDA) assay to evaluate oxidative stress associated with conessine treatment. Furthermore, molecular docking studies were conducted to assess the efficacy of conessine in binding to apoptotic regulatory proteins (Bcl-2 and Bax). **Results:** Conessine exhibited dose-dependent cytotoxicity in HCT116 cells, with an IC_{50} dose of 76.949 µg/mL resulting in a marked increase in apoptosis. Flow cytometric analysis revealed a significant twofold decrease in viable cells and a sevenfold increase in apoptotic cells compared with the untreated group. Dual staining further differentiated the apoptotic stages through characteristic morphological alterations, including chromatin condensation and nuclear fragmentation. The comet assay demonstrated a remarkable induction of DNA fragmentation in HCT116 cells. Enhanced 2′,7′-dichlorodihydrofluorescein fluorescence accumulation in conessine-treated cells indicated the induction of oxidative stress. Molecular docking analysis demonstrated favourable binding interactions between conessine and regulatory proteins. **Conclusion:** The results demonstrated that conessine induces apoptotic cell death in HCT116 cells and is associated with increased intracellular ROS and DNA damage. The integrated experimental and computational evidence highlights conessine as a promising novel candidate for CRC therapy, necessitating further comprehensive mechanistic and *in vivo* studies.

Keywords: Anticancer, Colon cancer, HCT116 cells, Phytochemicals, Regulatory proteins.

Correspondence:
Dr. Maryam Ahmed Halawi
Pharmacy Practice Research Unit,
Department of Pharmacy Practice,
College of Pharmacy, Jazan University,
Jazan, SAUDI ARABIA..
Email: marihalawi@jazanu.edu.sa

Received: 09-07-2026;
Revised: 24-08-2026;
Accepted: 12-10-2026.

INTRODUCTION

Colorectal Cancer (CRC) impacts the large intestine and rectum, ranking as the third most common cancer and second largest cause of cancer-associated mortality, mainly among individuals over 65 years of age.[1] The incidence rate of CRC is growing annually by 3% among younger adults aged 20-49 years, due to lifestyle alterations, genetic susceptibility, and environmental factors.[2] Numerous modern advances in cancer therapy, encompass ablation, targeted therapies, stem cell treatments, natural antioxidants, nanoparticles, sonodynamics, radionics, chemodynamics, and ferroptosis-based therapies, have been developed and are frequently used in cancer treatment, contributing to reduce the severity of cancer to some extent.[3] Still, the quest for natural substances continues to progress, owing to the availability of diverse medicinal properties and a growing concern for safety.[4] Phytochemicals such as resveratrol, lycopene, genistein, epigallocatechin gallate, and curcumin, have been reported to exhibit anticancer effects by targeting apoptosis, inflammation, oxidative stress, and tumor progression pathways.[5]

This study utilised a plant-derived alkaloid called conessine, found in *Holarrhena antidysenterica*, which is extensively studied

DOI: 10.5530/ijper.20270127

Copyright Information :
Copyright Author (s) 2027 Distributed under Creative Commons CC-BY 4.0

Publishing Partner : Manuscript Technomedia. [www.mstechnomedia.com]

for its antimicrobial, anti-inflammatory, antioxidant efficacies; however, its anticancer efficacy, especially in CRC, remains unexplored.[6] This work was undertaken to evaluate the anticancer characteristics of conessine, contemplating the effectiveness of alkaloids to influence mitochondrial pathways, promote oxidative stress, and regulate essential apoptotic proteins. Dysregulated apoptosis enables the uncontrolled proliferation of cancer cells and tumor progression; hence the induction of apoptosis is considered a key therapeutic strategy in cancer treatment. Elevated levels of ROS can disrupt the redox balance, which leads to DNA damage and later triggers apoptosis.[7] Previous studies show that phytochemicals can induce cytotoxicity in HCT116 cells via ROS-dependent mechanisms, which results in activating the intrinsic apoptotic pathways.[8]

In this context, the present study was designed to investigate the apoptotic potential of conessine using HCT116 human CRC cells. Comprehensive approaches involving the MTT assay, ROS analysis, flow cytometry, and fluorescence-based dual staining have been performed to observe morphological changes associated with apoptosis. Additionally, conessine's interactions with key apoptotic regulators such as Bcl-2 and Bax proteins have been studied using molecular docking analysis. This study integrates cellular and computational analyses to investigate the cytotoxic, apoptotic, oxidative-stress-associated, and DNA-damaging effects of conessine and to explore its potential interactions with apoptosis-associated proteins.

MATERIALS AND METHODS

Preparation of cell lines and chemicals

The cell line used in this study was procured from the National Centre for Cell Sciences (NCCS), Pune, India. Dulbecco's Modified Eagle's Medium (DMEM) and the other chemicals are bought from Sigma-Aldrich (USA) and Merck (Germany), respectively. Normal melting point agarose (NMPA) used in the comet assay was procured from Invitrogen, USA. The Human Colon Cancer Cell Line (HCT116) was cultured in Tissue culture flasks (25 cm^2) consisting of DMEM supplemented with Fetal Bovine Serum (FBS) (10%), sodium bicarbonate, L-glutamine, and antibiotics such as penicillin (100 U/mL), amphotericin B (2.5 µg/mL), and streptomycin (100 µg/mL). The HCT116 cultures were incubated at 37°C in a humidified atmosphere under 5% CO_2. 100 µL of trypsinised confluent monolayer cells, which contained 5×10^3 cells, was seeded into a 96-well tissue culture plate, and cell attachment was encouraged by incubation for 24 hr under standard culture conditions. Conessine was prepared in DMSO, and the final concentration of 0.1% was maintained in the treatment wells. To perform the cytotoxicity assay, 15 mg of MTT was dissolved in 3 mL of Phosphate-Buffered Saline (PBS) and sterilised by filtration. The cell lysis solution was prepared following the protocol described by Azqueta *et al.*[9] The phase-contrast microscope and inverted fluorescence microscope used in this study were Olympus CKX41 model equipped with Optika Pro5 CCD camera. The Fluorimeter was purchased from Qubit 3.0, Life Technologies, USA.

Cytotoxic Evaluation by MTT Assay

Conessine at varying doses (6.25, 12.5, 25, 50, and 100 µg/mL) was loaded into the 96-well plate containing the overnight-grown HCT116 culture and incubated for 24 hr. Morphological changes induced by cytotoxic effects of conessine on HCT116 cells were observed using a phase-contrast microscope. For quantitative evaluation, the MTT assay was carried out as described by Boyraz *et al.* with a few modifications.[10] Old growth medium in the culture wells were replaced with 30 µL of MTT solution and allowed for formazan crystal formation under incubation (4 hr). Crystals dissolved in DMSO were used for the determination of cell viability using a microplate reader at an absorbance of 540 nm.

$$\text{Cell viability (\%)} = \frac{\text{Mean OD of the test}}{\text{Mean OD of control}} \times 100$$

The Half-Maximal Inhibitory Concentration (IC_{50}) of conessine was determined using ED_{50} PLUS V1.0 software.

Apoptosis Study by Annexin V-FITC/PI Flow Cytometry

Apoptosis was evaluated using the Dead Cell Apoptosis Kit, which includes recombinant annexin V conjugated to fluorescein (Alexa Fluor-488) and a prepared solution of the red-fluorescent Propidium Iodide (PI) nucleic acid binding dye. Cell pellets (1×10^6 cells) of Conessine (IC_{50})-treated HCT116 cells were resuspended in 100 µL of Muse™ Annexin V and Dead Cell reagent.[11] Annexin V is a calcium-dependent phospholipid-binding protein that has a high affinity for phosphatidylserine on apoptotic cells, thereby distinguishing HCT116 cells at different stages of apoptosis. A flow cytometer owned by the Muse™ Cell Analyser, using the 488 nm line of an argon-ion laser, acquires data based on the excitations as follows: apoptotic cells with green fluorescence, dead cells with red and green fluorescence, and live cells with little or no fluorescence. Cells were gated based on forward and side scatter to exclude debris, and fluorescence compensation was applied where necessary. Apoptotic cells were quantified using Muse FCS 3.0 software, and the percentage distribution in each quadrant was calculated. Comparison between the treated and control groups determined the apoptotic effect of conessine.

Determination of Apoptosis by Fluorescence-based Dual Staining

Acridine Orange (AO) and Ethidium Bromide (EtBr) dual staining is a fluorescence technique intended to differentiate viable, apoptotic, and necrotic cells based on membrane integrity and nuclear morphology. The AO/EtBr staining method was performed as described previously by Alshehade *et al.* with minor modifications.[11] Conessine (IC_{50}) treated HCT116 cells were

stained using a freshly prepared AO and EtBr mixture in a 1:1 ratio and incubated in the dark for 10 min to ensure successful staining. A small aliquot of the cell suspension was placed on a clean glass slide for microscopic analysis using a fluorescence microscope equipped with a blue filter. Viable cells are observed with uniform green nuclei with intact structure; early apoptotic cells with bright green nuclei and chromatin condensation or fragmentation; late apoptotic cells with orange to red nuclei and condensed or fragmented chromatin; and necrotic cells are observed with orange/red nuclei without distinct chromatin condensation.

Comet assay

Conessine (IC_{50}) treated (as described above) HCT116 cells (1×10^4 cells) were trypsinised and resuspended in 10 µL of Low-Melting-Point Agarose (LMPA) in 6-well plates. This LMPA mixture was layered over the frosted (4°C) slides already coated with 1% NMPA, and the slides were further solidified at 4°C and a coverslip was placed over them. Finally, both agarose layers were covered with sterile NMPA, and incubated for 20 min at 4°C. The slides were immersed in a cold cell lysis solution and kept at 4°C for 2 hr to lyse the cells and release the DNA nucleoids. Following lysis, DNA unwinding was performed in alkaline electrolysis buffer at 25 V and 300 mA for 20 m. 0.4 M Tris buffer (pH 7.5) was used three times to neutralise, and stained with 20 µg/mL of EtBr.[12] Images of comets captured using an inverted epifluorescence microscope were analysed with Tritek comet scoring software to measure DNA damage.

Determination of Intracellular Reactive Oxygen Species (ROS) Using DCFDA Assay

This assay uses 2',7'-Dichlorodihydrofluorescein Diacetate (DCFDA), a fluorogenic dye that is oxidised by ROS and forms 2',7'-Dichlorofluorescein (DCF). DCFDA solution (50 µL) was added to conessine-treated HCT116 cells at 60% confluency. Fluorescence microscope with a blue filter was used to capture the images and Fluorimeter (Qubit 3.0, Life Technologies, USA) with excitation at 470 nm and emission at 635 nm was used to quantify colour intensity. The fluorescence intensity is directly proportional to the level of intracellular ROS and the values were expressed in Arbitrary Units (AU).

Molecular Docking Analysis

The three-dimensional X-ray crystallographic structure of proteins: (a) Bcl-2 (ID: 6O0K) with the crystallographic resolution 1.62 Å; (b) BAX (ID: 1F16); Conessine (ID: 441082); and reference inhibitors: Venetoclax (ID:49846579) and BAM7 (ID:3101542), was downloaded from the Research Collaboratory for Structural Bioinformatics (RCSB) Protein Data Bank (PDB), and the necessary alterations were implemented. The peptide chain lengths of 166 and 196 amino acids have been reported for BCL-2 and BAX, respectively.

With the help of Discovery Studio v. 25, insertion, removal, standardisation, and energy minimisation have been carried out on the proteins and variations of the ligand (retrieved from PubChem database) were optimised by modifying the structure. Studio v.25 forecasts protein binding sites using PDB site information, which aids in understanding the molecular interactions. The LibDock protocol identifies the ligand conformations within the protein active site based on polar interactions (hotspots), and the CHARMM force field determines the energy and forces acting on each particle.[13] The LibDock module generated a total of 30 docked poses for the selected ligands within the defined binding site of Bcl-2 and Bax. LibDock scores reflect the geometric and energetic compatibility of the ligand within the receptor binding pocket.

Statistical Analysis

Each experimental condition was assessed in triplicate wells, and results are presented as mean±SD. The values were analyzed for statistical comparison using GraphPad Prism 5.1. The values were subjected to one-way ANOVA, and the groups were compared using Tukey's multiple comparison test. $p<0.05$ was considered significant.

RESULTS

Cytotoxicity induced by conessine

The results of the cytotoxicity assay demonstrated a dose-dependent inhibition of cell viability after 24 hr of treatment with varying concentrations of conessine. Morphological observations using an inverted phase-contrast microscope revealed the typical adherent morphology of the untreated HCT116 cells, with intact cell membranes and uniform distribution (Figure 1A). In contrast, conessine-treated cells (Figures 1B-1F) displayed progressive morphological alterations with increasing concentrations, including cell detachment from the surface, cytoplasmic granulation, cell rounding, shrinkage, and formation of cellular debris. Extensive cell death and loss of integrity were clearly observed at higher doses of 50 and 100 µg/mL (Figures 1E and 1F). The quantitative result of the MTT assay is depicted in Figure G, which supports the morphological observations. HCT116 cells treated with 6.25 µg/mL conessine showed a slight reduction in viability (90 - 95%), whereas a marked decrease in viability (60 - 65%) was evidenced at 50 µg/mL concentration, and a substantial reduction to 35 - 40% viability was observed at 100 µg/mL. The IC_{50} value was 76.949 µg/mL. Statistical analysis indicated a significant (***$p<0.001$) reduction in cell viability across all tested concentrations compared with the control.

Conessine-induced Apoptotic and Associated Morphological Variations

Figure 2 shows the flow cytometry results obtained for the control and test (treated with IC_{50} of conessine). In the untreated group

(Figure A), approximately 93.10% of the cell population remained live, and 6.9% had undergone apoptosis. In contrast, conessine treatment (Figure B) significantly altered the distribution, with the percentage of viable cells markedly decreased to approximately 49.15% and the apoptotic cells increased to 50.85%. The graphical representation (Figure C) further confirmed these findings, showing a significant difference (*p<0.05) recorded in the viability of HCT116 cells treated with conessine.

Fluorescence-based Dual Staining Marked Different Stages of Apoptosis

The predominant green fluorescence observed in Figure 3A indicates high cell viability, intact membrane integrity, and normal nuclear morphology in untreated cells. Conversely, conessine-treated cells (Figure B) exhibited noticeable morphological alterations indicative of apoptosis. A significant proportion of cells displayed intense green fluorescence alongside condensed or fragmented chromatin, signifying early apoptosis. Additionally, a significant number of cells exhibited orange-to-red fluorescence with nuclear condensation and fragmentation, representing late apoptosis or necrosis. The progression of apoptosis and loss of membrane integrity in HCT116 cells was indicated by the appearance of intensely red/orange-stained cells. A marked reduction in cell viability was noted in conessine-treated cells (45-50%) compared to untreated HCT116 cells (95-98%). Simultaneously, there was a significant increase in early apoptotic (15-20%) and late apoptotic cells (30-35%) following conessine treatment. The observed alterations were statistically significant (**p<0.01) compared to the untreated group.

Conessine Induces DNA damage

The fluorescence image of comet formation in Figure 4A displayed minimal comet tail formation, indicating negligible DNA damage and preservation of genomic integrity in untreated HCT116 cells. In contrast, pronounced comet formation was characterised by increased tail length and intensity in conessine-treated cells, reflecting extensive DNA strand breaks (Figures 4A and 4B). The mean length of the comet has been significantly (p<0.01) increased from 15 - 18 to 115 - 120 µm from untreated to conessine-treated cells (Figures 4C and 4D).

Oxidative Stress Damages the Cell Structure and Integrity

Phase contrast and fluorescence images (Figure 5A) showed minimal green fluorescence, indicating low basal ROS levels and normal cellular redox status in the control group. In addition, untreated HCT116 cells maintained the typical morphology and uniform distribution. On the contrary, the significantly (p<0.01) higher rate of green fluorescence displayed in the conessine-treated group, between 12,500 and 13,000 AU, compared to the low rate of approximately 1000 AU in control cells (Figure B). Enhanced DCF fluorescence accumulation in

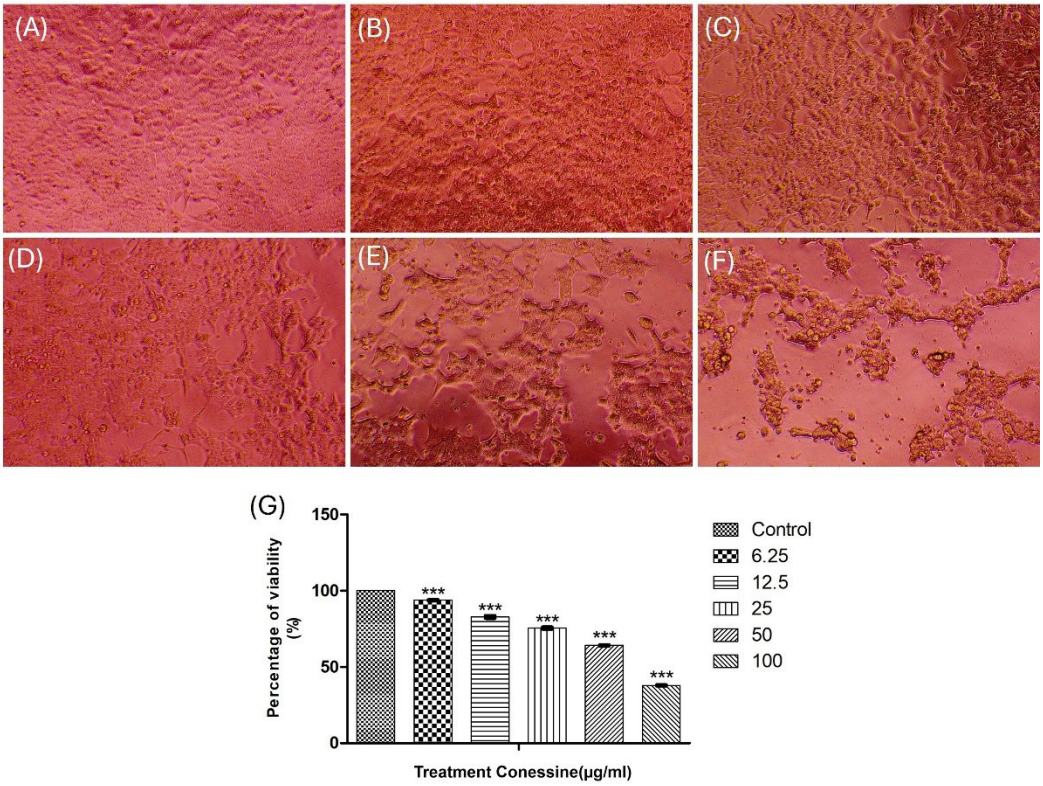


Figure 1: Effect of conessine on HCT116 cell viability. (A) Control cells showing normal morphology; (B-F) cells treated with increasing concentrations of conessine (6.25-100 µg/mL) showing morphological changes indicative of cytotoxicity. (G) Graph representing percentage cell viability after 24 hr treatment, showing a dose-dependent decrease. Values are expressed as mean±SD from triplicate measurements (n=3); ***p<0.001 vs control.

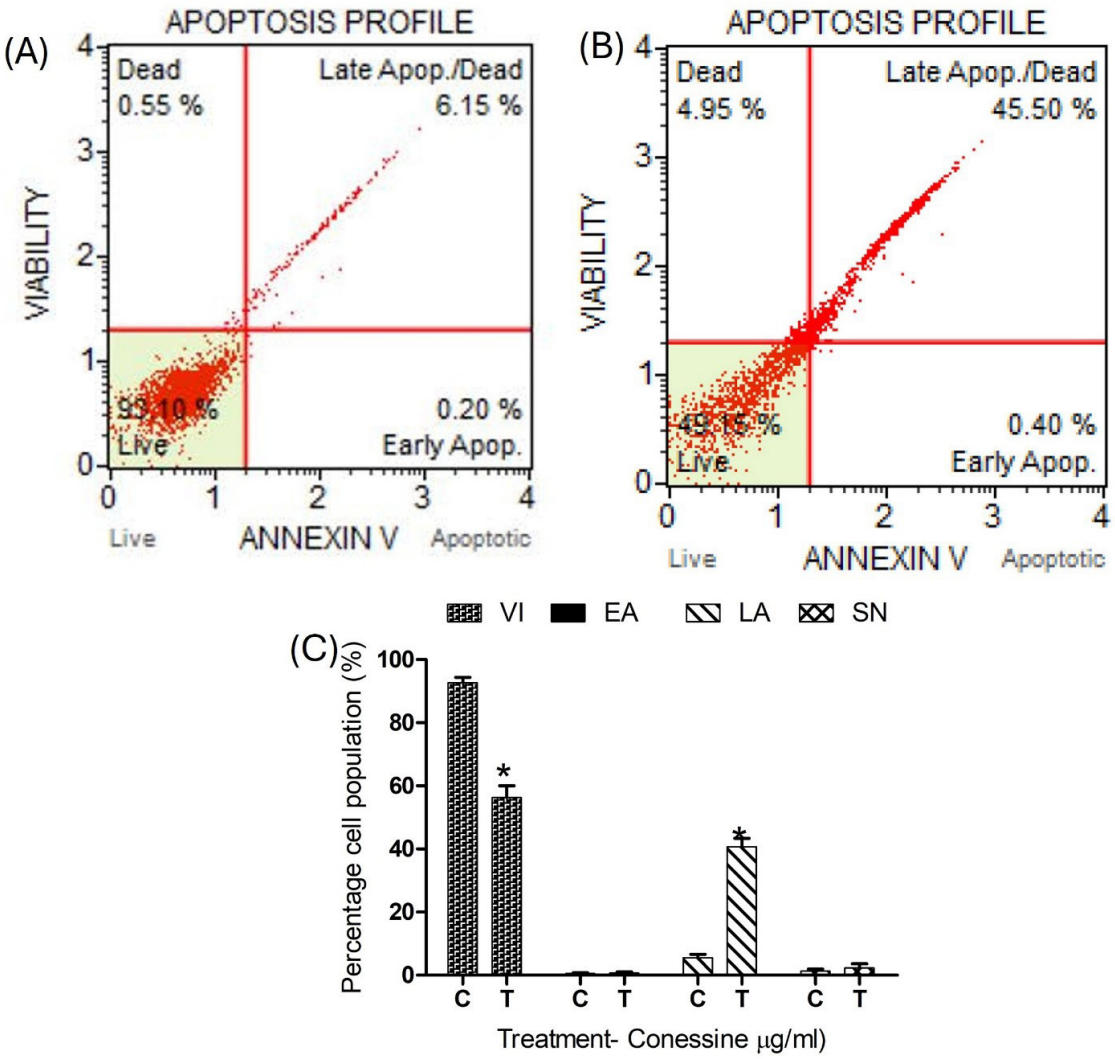


Figure 2: Annexin V-FITC/PI (Propidium iodide) flow cytometric analysis of apoptosis in HCT116 cells. (A) Control cells showing predominant viable population; (B) Conessine-treated cells showing increased apoptotic population; (C) Quantitative analysis of viable (VI), Early Apoptotic (EA), Late Apoptotic (LA), and Secondary Necrotic (SN) cells. Values are expressed as mean±SD from triplicate measurements (n=3); *p<0.05 vs control.

treated cells suggested oxidative stress induction. In addition, several remarkable morphological alterations consistent with oxidative damage have been observed, including cell shrinkage, detachment, and loss of monolayer integrity.

Molecular Docking

Docking with BCL-2

LibDock scores, the interacting residues, the type of the interaction bond and the bond distance are tabulated for Bcl-2 (Table 1). LibDock scoring algorithm indicated a strong binding affinity of conessine within the active site of the target protein, with a score of 93.0517 relative to 131.076 of Venetoclax. Additionally, the binding affinity and specific polar interactions are stabilised by numerous hydrogen-bond interactions, especially those involving the ASP111 and GLU136 residues, with bond distances ranging from approximately 2.51747 to 2.79506 Å. The hydrophobic interactions formed with MET115, VAL133, LEU137, ALA149, PHE104 and PHE112 residues are recognised as contributors to the overall stability of the ligand-protein complex (Figure 6). Venetoclax, the reference inhibitor, formed many hydrogen bonds with key active-site residues, including ASN143, ARG146, and ASP14, with bond distances below 4.0 Å, indicating strong interactions. MET115, ALA149, VAL133, VAL156, PHE104 and ARG146 residues formed robust hydrophobic interactions, which enhance the binding efficiency of venetoclax within the catalytic pocket.

Docking with BAX

Conessine exhibited a LibDock score of 58.5763, indicating a favourable binding affinity within the active site of the target protein, relative to the LibDock score of BAM7 (score:115.999). The hydrogen-bond interactions are formed by the residues VAL180, ASP102, MET99, ASP102 and ASN104, with bond distances below 3.0 Å (Table 2). The hydrophobic interactions

observed for BAX include ARG109, VAL180, and ARG109, which are likely to contribute to the overall stability of the ligand-protein complex (Figure 7). The reference inhibitor, BAM7, forms hydrogen bonds with SER101, ARG147 and ASN104, with bond distances below 3.0 Å, indicating an efficient interaction. A formal redocking/RMSD validation procedure was not performed in the present computational workflow. Therefore, the docking results are interpreted as predictive computational evidence rather than experimentally validated binding interactions.

DISCUSSION

Natural plant-derived compounds (phytochemicals) play a dual role in regulating apoptosis, serving as either pro-apoptotic to eliminate malignant cells or anti-apoptotic agents to safeguard healthy cells, contingent upon the cellular context and disease condition.[14] The phytochemicals induce apoptosis in cancer cells by various mechanisms, including elevation of intracellular ROS, modulation of key apoptotic regulators, and inhibition of pro-survival signaling pathways.[15] The ability of phytochemicals to regulate the equilibrium between pro- and anti-apoptotic signals is crucial for maintaining cellular homeostasis and shielding normal cells from damage.[16] Consequently, natural compounds have gained significant attention as therapeutic agents for cancer and other diseases characterised by excessive apoptosis. This study examined the antiapoptotic efficacy of conessine in HCT116 human colon cancer cells using analyses, including cytotoxicity, apoptosis, ROS, DNA damage, and molecular docking using Bcl-2 and BAX proteins. The MTT assay determined the IC_{50} of conessine to be 76.949 µg/mL, confirming its efficacy as an inhibitory dose for HCT116 colon cancer cells. HCT116 cells showed morphological alterations, including loss of adhesion, cytoplasmic granulation, cellular reconfiguration, and formation of cellular debris. Previous studies showed that curcumin at an LC_{50} of 30 µM displayed comparable apoptotic characteristics, including membrane blebbing in HCT116 cells.[17] Sericin-urea, a silk protein extracted from *Bombyx mori*, exhibited cytotoxicity on HCT116 cells with an IC_{50} of 42.00 ± 0.002 µg/mL, but this study did not investigate the morphological alterations.[18] Morphological alterations provide visual evidence of apoptosis, aligning with underlying molecular events such as oxidative

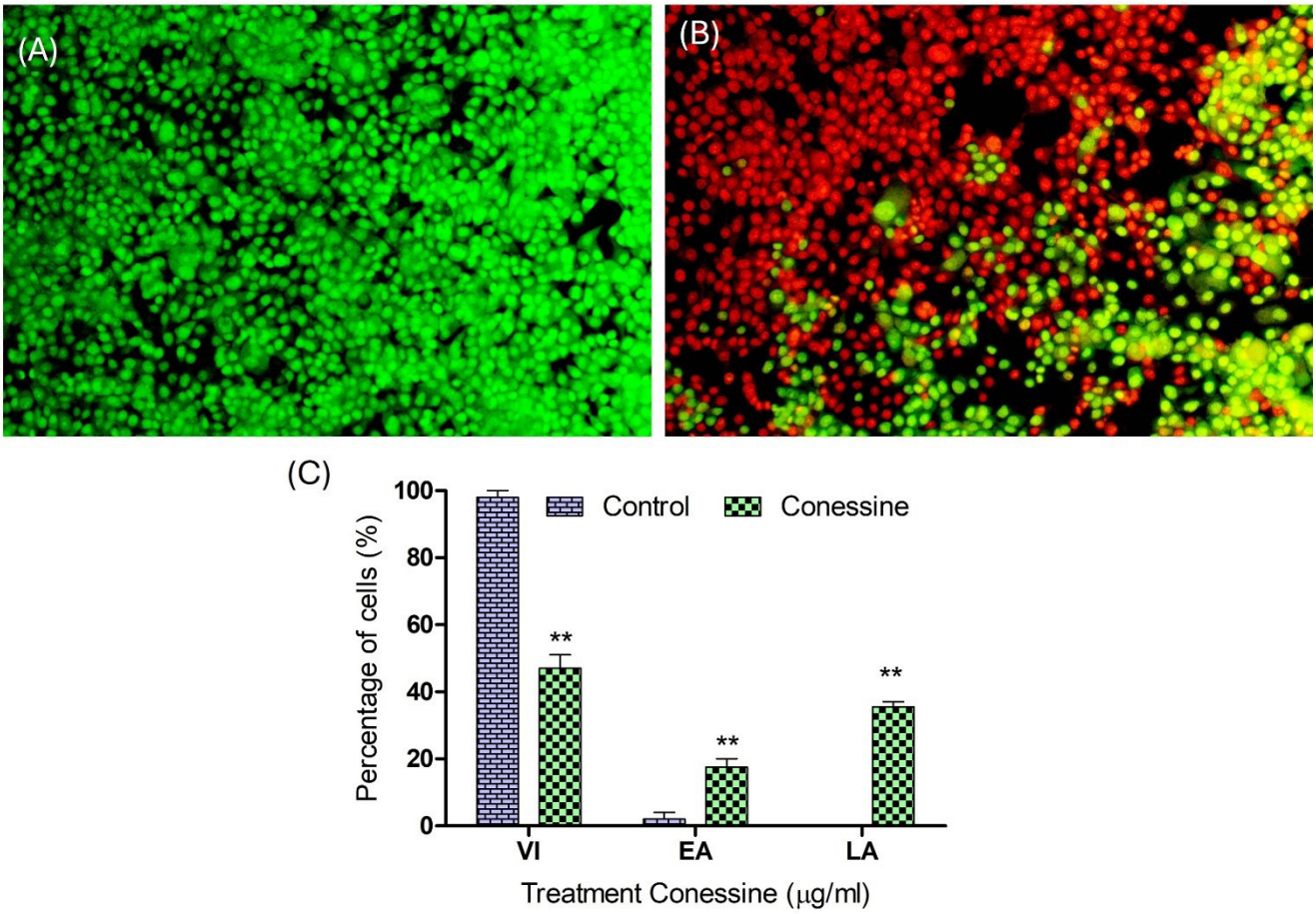


Figure 3: (Panel 3C (quantitative analysis) is captioned but not explicitly cited by panel label in the Results text (only prose percentages given). Acridine Orange/Ethidium Bromide (AO/EtBr) dual staining of HCT116 cells. (A) Control cells showing viable cells with uniform green fluorescence; (B) Conessine-treated cells showing high rate of apoptotic cells with green (early apoptosis) and orange/red (late apoptosis) fluorescence; (C) Quantitative analysis of Viable (VI), Early Apoptotic (EA), and Late Apoptotic (LA) cells. Values are expressed as mean±SD from triplicate measurements (n=3); **p<0.01 vs control. Panel 3C (quantitative analysis) is described in the legend but not explicitly cited by panel label in the Results text (only prose percentages given).

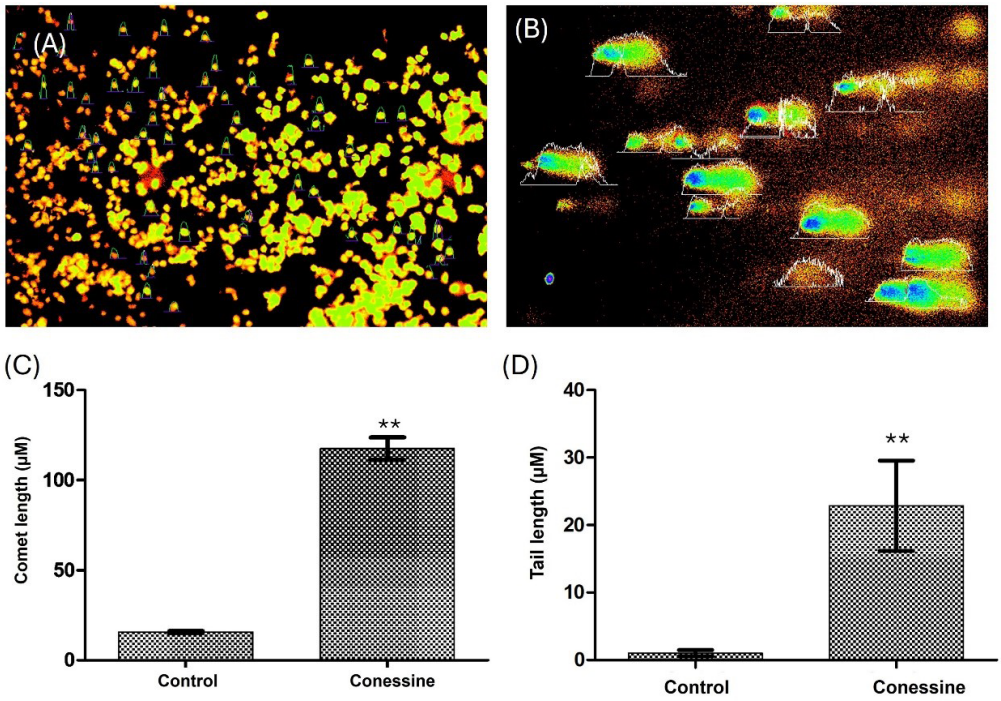


Figure 4: Comet assay analysis of DNA damage in HCT116 cells. (A) Control cells showing intact nuclei with minimal tail formation; (B) Conessine-treated cells showing pronounced comet tails indicating DNA damage; (C) Quantitative analysis of comet length; (D) Quantitative analysis of tail length. Values are expressed as mean±SD from triplicate measurements (n=3); **p<0.01 vs control.

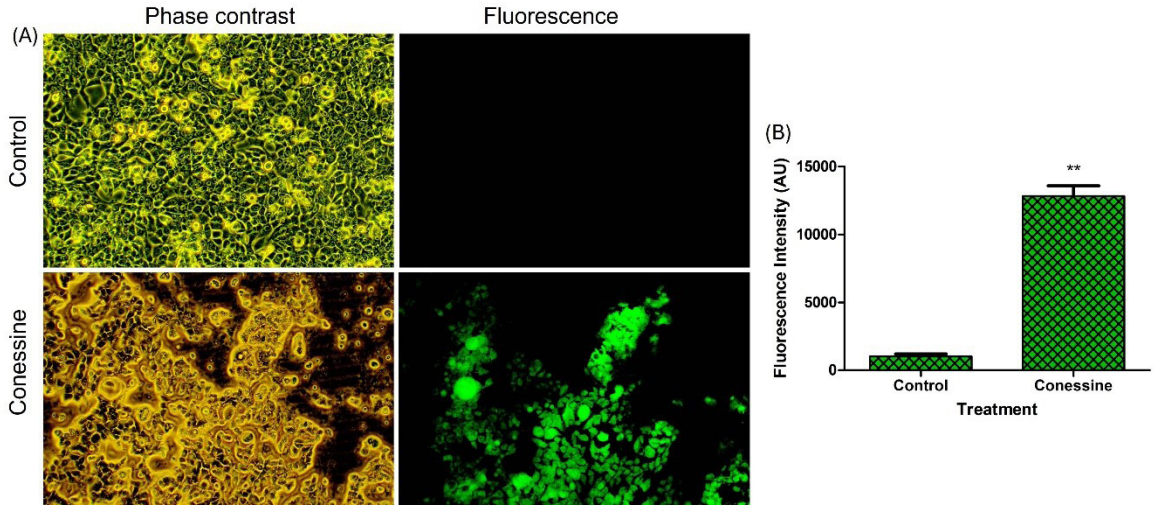


Figure 5: (Suggestion: Figure count exceeds the standard limit of 4 - see Author Query regarding Figure limit). Reactive Oxygen Species (ROS) generation in HCT116 cells using 2′,7′-Dichlorodihydrofluorescein Diacetate (DCFDA) assay. (A) Phase contrast and fluorescence images of control and conessine-treated cells showing increased green fluorescence in treated cells; (B) Quantitative analysis of fluorescence intensity. Values are expressed as mean±SD from triplicate measurements (n=3); **p<0.01 vs control.

stress and DNA fragmentation, thereby confirming the cytotoxic potential.

A study on apoptosis is crucial for validating the anti-cancer potential of a compound because it provides cellular-level insight. We confirmed the apoptotic characteristics of conessine by Annexin V-FITC/PI flow cytometry and AO/EtBr dual staining. The proportion of apoptotic cells increased significantly to 50.85% upon conessine treatment, compared with 6.9% recorded in the untreated control group. Additionally, classical apoptotic characteristics such as chromatin condensation, membrane blebbing, and nuclear fragmentation have been recorded, indicating a conessine-driven irreversible apoptotic stage rather than transient early apoptosis. Combinations of *Coix lacryma-jobi*, an Asian herb commonly used in Chinese medicine, and sorafenib, an oral anticancer agent, demonstrated an early apoptotic efficacy of around 15% when administered separately, and around 25% when used as a mixture, with doses of 1000 µg/mL and 1 µmol/L for each compound, respectively.[19]

In comparison to the above study results, conessine exhibited significant apoptotic efficacy at 76.949 µg/mL concentration. A previous study by Chen and Men demonstrated that artemetin, a flavonoid, induces apoptosis in HCT116 cells at an IC_{50} of 5 µg/mL. AO/EB dual staining, which showed increased yellow and orange fluorescence, indicating early and late apoptosis, respectively.[20] The study reported a notable rise in total apoptotic cell population (65-70%) compared to control (30-35%) after artemetin treatment; nevertheless, it relied on fluorescence-based qualitative assessment without accurate quantification of apoptotic phases.

The genotoxicity potential of conessine has been evaluated using the comet assay, which provides strong evidence of the intensity of DNA damage caused by the anticancer compound.[21] Conessine treatment significantly increased the tail length, measuring between 115 and 120 µm, indicative of extensive DNA fragmentation. Quercetin-loaded Selenium Nanoparticles (Qu-SeNPs) induced DNA damage in HCT 116 cells by about eightfold compared to the control group. The values were approximately 15.7 µm for 51 µg/mL Qu-SeNPs and roughly 12.3 µm for the cisplatin reference drug (18 µg/mL).[22] Mahmoud *et al.* observed that methanolic extracts of medicinal plants named *Quercus robur* and *Ononis vaginalis* induce DNA

Table 1: Interactions between Bcl-2 with conessine and reference inhibitor venetoclax.

Sl. No.	Ligands	LibDock Score	Interacting Residue	Bond Distance	Bond Nature
1.	Conessine (PubChem ID: 441082)	93.0517	441082:H58 - A:ASP111:O	2.51747	Hydrogen Bond
			441082:H60 - A:GLU136:O	2.79506	Hydrogen Bond
			A:MET115 - 441082	5.24866	Hydrophobic
			A:VAL133 - 441082	5.18042	Hydrophobic
			A:LEU137 - 441082	5.34903	Hydrophobic
			A:LEU137 - 441082	4.18803	Hydrophobic
			A:LEU137 - 441082	5.244	Hydrophobic
			A:ALA149 - 441082	4.48001	Hydrophobic
			441082:C19 - A:VAL156	5.05821	Hydrophobic
			A: PHE104 - 441082:C19	5.06692	Hydrophobic
			A: PHE112 - 441082:C19	4.19405	Hydrophobic
2.	Venetoclax (Pubchem ID:49846579)	131.076	A:ARG146:NH1 - 49846579:O8	5.04167	Electrostatic
			A:ASN143:HD21 - 49846579:O7	2.51042	Hydrogen Bond
			A:ASN143:HD22 - 49846579:O7	2.31667	Hydrogen Bond
			A:ARG146:HH12 - 49846579:O9	2.7006	Hydrogen Bond
			49846579:H62 - A:ASP140:O	2.86599	Hydrogen Bond
			A:ARG146:NH1 - 49846579	3.66587	Electrostatic
			A: ARG146: HE - 49846579	3.15726	Hydrogen Bond
			A: PHE104:HD1 - 49846579	2.78016	Hydrophobic
			A:MET115 - 49846579	5.18329	Hydrophobic
			A:ALA149 - 49846579:C24	4.44963	Hydrophobic
			A:ALA149 - 49846579	4.354	Hydrophobic
			49846579:Cl1 - A:VAL133	4.16267	Hydrophobic
			49846579:Cl1 - A:LEU137	5.20601	Hydrophobic
			49846579:C25 - A: VAL156	3.88317	Hydrophobic
			A: PHE104 - 49846579	5.15918	Hydrophobic
			A: PHE104 - 49846579:C24	4.17364	Hydrophobic
			A: PHE104 - 49846579	5.23238	Hydrophobic
			A: PHE112 - 49846579:C25	4.50021	Hydrophobic
			49846579 - A: MET115	5.02246	Hydrophobic
			49846579 - A:VAL133	4.76257	Hydrophobic
			49846579 - A:LEU137	5.09218	Hydrophobic
			49846579 - A:ARG146	4.69404	Hydrophobic

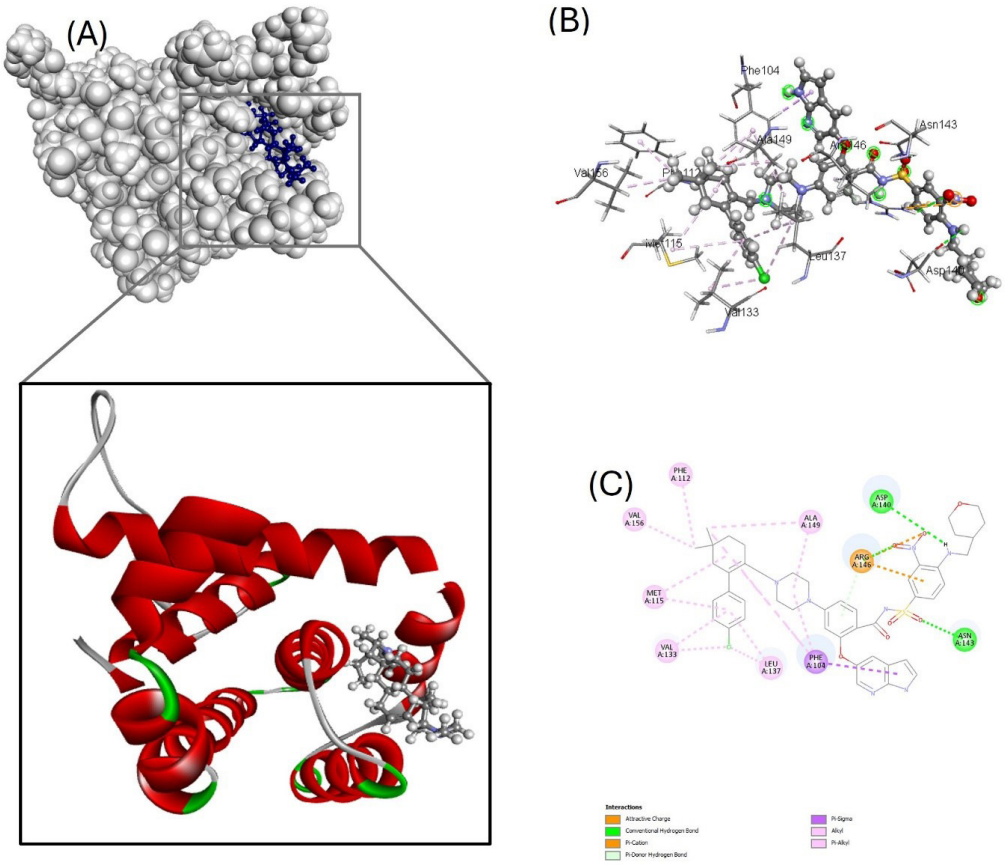


Figure 6: Bcl-2 docking with conessine. (A) The surface representation of protein [Protein databank ID: 6O0K] ligand Complex; (B and C) Three and two-dimensional representation of the interaction between the ligand and the target.

damage in HCT116 cells, evidenced by the comet tail lengths of 26.50±0.65 AU and 18.0±1.2 AU, respectively.[23] The present study provides quantitative measurements in micrometres, indicating a higher-resolution assessment of DNA fragmentation caused by conessine. Recent reports have demonstrated that elevated tail length and DNA migration following treatment with anticancer compounds indicate the induction of genotoxic stress, consequently reducing cancer cell viability and triggering apoptosis.[24] These observations suggest that oxidative stress may be associated with the observed DNA damage and apoptosis; however, the specific signaling pathway responsible for these effects remains to be elucidated.[25]

Phase contrast and fluorescence microscopy demonstrated the potential efficacy of conessine in inducing oxidative stress and associated morphological alterations. The qualitative and quantitative measurements obtained from DCFH-DA fluorescence analysis demonstrated a high rate of green fluorescence (12,500-13,000 AU) and remarkable morphological alterations compared with the untreated group (approximately 1000 AU). According to the report of Soumya *et al.*, the petroleum ether extract of *Curcuma mutabilis* rhizome at 5.5 µg/mL (IC_{50}) enhanced around a threefold increase in ROS levels in HCT116 cells.[26] A similar ROS-mediated cytotoxic mechanism has been reported in HCT116 cells, following the treatment of *Jania rubens*, a Lebanese seaweed rich in flavonoid and pyrazole derivatives. Approximately a seven- to eightfold increase in ROS levels has been noted for the 250-500 µg/mL extract.[27] Elevated oxidative stress is a critical factor leading to antiproliferative effects and the alteration of epigenetic regulatory mechanisms.[28]

Molecular docking analysis provided additional computational evidence for potential interaction of conessine and apoptosis-associated proteins such as BAX and Bcl-2. Conessine formed predicted hydrogen-bond and hydrophobic interactions within the respective binding regions of these proteins. Conessine exhibited significant binding affinity with key amino acid residues of Bcl-2 via hydrogen bonding and hydrophobic interactions, with a score of 93.0517 relative to 131.076 for Venetoclax. The effectiveness of binding was confirmed by the stabilisation achieved by significant hydrogen (ASP111 and GLU136) and hydrophobic (MET115, VAL133, LEU137, and PHE) interaction residues. Hydrogen bonding and hydrophobic interactions are critical determinants of ligand stability in Bcl-2 binding pockets.[29] In the present study, conessine demonstrated a LibDock score of 58.57, which is lower than that of the reference

inhibitor BAX (−7.54 kcal/mol). The presence of hydrogen bonds with the VAL180, ASP102, and ASN104 residues, and hydrophobic interactions with ARG109, VAL180, and ARG109 residues, supports conessine's interaction with the pro-apoptotic protein. In a study by Parveen *et al.*, piperlongumine docked with BAX, exhibiting a binding energy of −7.54 kcal/mol, where the binding was mainly driven by hydrophobic interactions rather than hydrogen bonding. Conessine demonstrated a LibDock score of 58.57 in the BAX docking analysis and formed predicted hydrogen-bond and hydrophobic interactions with residues within the binding region. These findings indicate a predicted interaction between conessine and BAX; however, LibDock scores should be interpreted within the scoring framework of the docking protocol and should not be directly compared with binding energies reported in kcal/mol from other studies. This study highlights that distinct interaction patterns can also effectively modulate BAX activity.[29] The tested apoptotic regulatory proteins are considered a critical determinant of cell fate. BCL-2 regulates the intrinsic apoptotic pathway by controlling mitochondrial membrane integrity, whereas BAX functions as a pro-apoptotic effector that promotes mitochondrial outer membrane permeabilisation, leading to cytochrome release and activation of the caspase cascade. Additionally, Bcl-2 acts as an anti-apoptotic protein by inhibiting BAX activation and preserving mitochondrial stability; an imbalanced BAX/Bcl-2 ratio decides the cell fate.[30] These findings support the possibility that BAX and Bcl-2 may be relevant to the cellular response to conessine; however, docking predictions alone cannot establish changes in protein expression, activation, or biological regulation. Experimental validation of these proteins and downstream apoptotic markers will therefore be necessary to confirm their involvement.

In this study, the observation from microscopy demonstrated a significant increase in apoptotic cell populations and nuclear fragmentation. The significant increase in intracellular ROS levels following conessine treatment indicates an association between oxidative stress and the observed cellular responses, including DNA damage and apoptosis.[31] However, further ROS-scavenging experiments can establish a direct connection

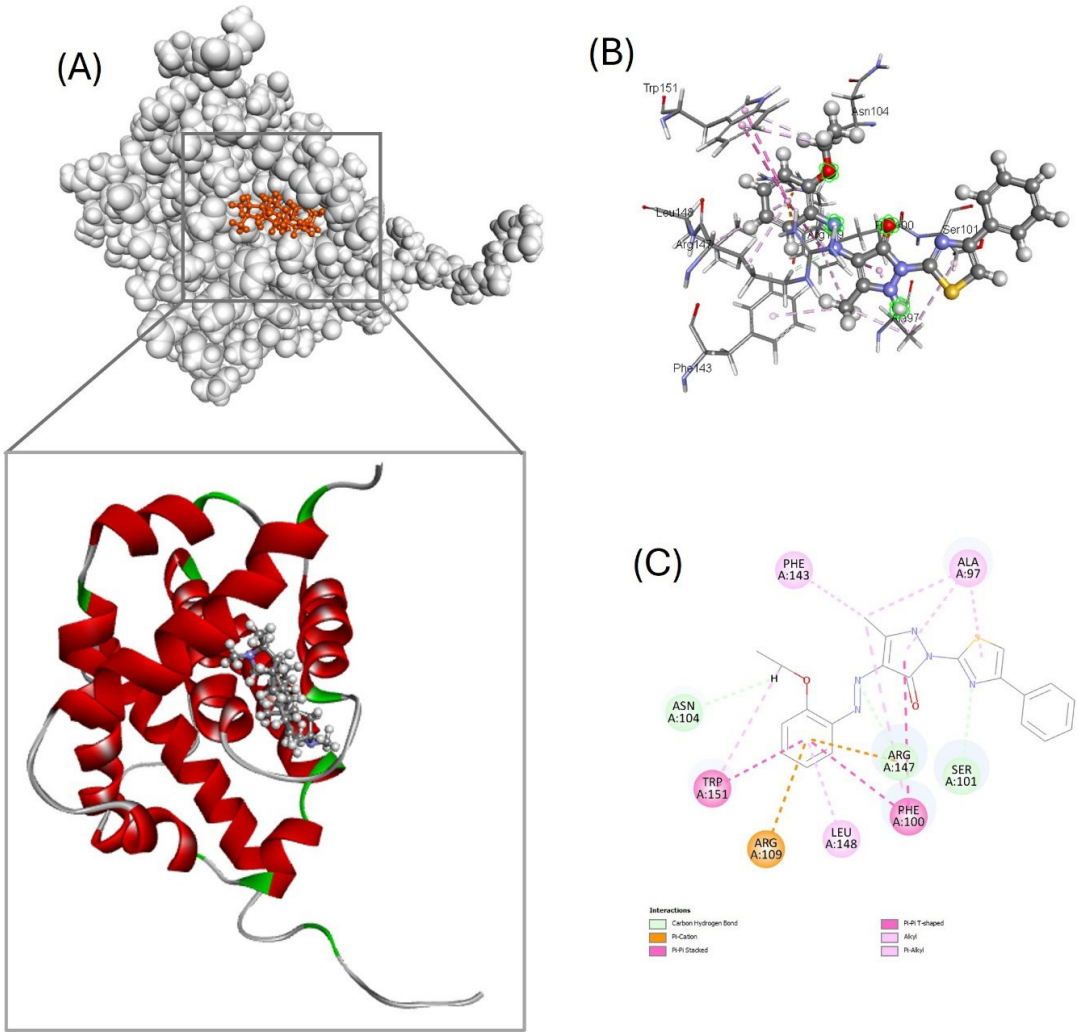


Figure 7: Bax docking with conessine. (A) The surface representation of protein [Protein Databank ID: 1F16] ligand Complex; (B and C) Three and two-dimensional representation of the interaction between the ligand and the target.

Table 2: Interactions between BAX with Conessine and reference inhibitor BAM7.

Sl. No.	Ligands	LibDock Score	Interacting Residue	Bond Distance	Bond Nature
1.	Conessine (PubChem ID: 441082)	58.5763	A:VAL180:HA - 441082:N1	2.91553	Hydrogen Bond
			441082:H60 - A:ASP102:O	2.02411	Hydrogen Bond
			441082:H61 - A:MET99:O	2.33583	Hydrogen Bond
			441082:H64 - A:ASP102:O	2.19008	Hydrogen Bond
			441082:H66 - A:ASN104:O	2.6278	Hydrogen Bond
			A:ARG109 - 441082	4.87225	Hydrophobic
			A:VAL180 - 441082	4.93356	Hydrophobic
			441082:C20 - A:ARG109	4.31923	Hydrophobic
2.	BAM7 (Pubchem ID: 3101542)	115.999	A:SER101:HA - 3101542:N6	2.31113	Hydrogen Bond
			A:ARG147:HD1 - 3101542:N7	2.5287	Hydrogen Bond
			3101542:H44 - A:ASN104:O	2.58405	Hydrogen Bond
			A:ARG109:NH1 - 3101542	4.27285	Electrostatic
			A:ARG147:NH1 - 3101542	3.52984	Electrostatic
			A:PHE100 - 3101542	4.86983	Hydrophobic
			3101542 - A:PHE100	5.76415	Hydrophobic
			A:TRP151 - 3101542	5.16798	Hydrophobic
			A:TRP151 - 3101542	4.63208	Hydrophobic
			A:ALA97 - 3101542:C13	3.92084	Hydrophobic
			A:PHE100 - 3101542:C13	5.28482	Hydrophobic
			A:PHE143 - 3101542:C13	4.09683	Hydrophobic
			A:TRP151 - 3101542:C28	4.473	Hydrophobic
			A:TRP151 - 3101542:C28	4.22618	Hydrophobic
			3101542 - A:ALA97	4.97824	Hydrophobic
			3101542 - A:ALA97	4.2396	Hydrophobic
			3101542 - A:ARG147	4.23264	Hydrophobic
			3101542 - A:LEU148	5.39811	Hydrophobic

between ROS generation and apoptosis. Although the observed apoptotic phenotype and the predicted interactions with Bcl-2 and BAX are compatible with involvement of apoptotic signaling, mitochondrial membrane depolarization, cytochrome c release, caspase activation, and PARP cleavage were not directly measured. Therefore, the involvement of the intrinsic mitochondrial apoptotic pathway should be regarded as a proposed mechanism rather than a demonstrated pathway.[32,33] The biological scope of the present study is also limited by the use of a single colorectal cancer cell line, HCT116. Future studies should therefore evaluate additional colorectal cancer models alongside normal colon epithelial cells to assess the reproducibility and specificity of the observed effects. Hence, the present findings should be interpreted as preliminary evidence obtained from an *in vitro* HCT116 cell model. Future studies providing information regarding pharmacokinetics, tissue distribution, systemic toxicity, or therapeutic selectivity, animal studies and subsequent translational investigations, will be necessary to determine the therapeutic relevance of conessine.

CONCLUSION

Taken together, the present findings provide preliminary *in vitro* evidence that conessine reduces HCT116 cell viability and is associated with increased oxidative stress, DNA damage, and apoptotic cell death via its potential interactions with Bcl-2 and Bax. However, the causal contribution of ROS and specific mitochondrial apoptotic signaling pathways were not directly established in the present study. Therefore, this study should not be interpreted as evidence of therapeutic efficacy. Further studies involving ROS-scavenging approaches, experimental validation of apoptotic signaling, additional colorectal cancer and normal colon cell models, and *in vivo* investigations are required to establish the mechanistic basis, selectivity, and therapeutic relevance of conessine.

ABBREVIATIONS

AO: Acridine Orange; **AU:** Arbitrary Units; **BAX:** Bcl-2-Associated X Protein; **BCL-2:** B-Cell Lymphoma 2; **CHARMM:** Chemistry at HARvard Macromolecular Mechanics; **CRC:** Colorectal Cancer;

DCFDA: 2′,7′-Dichlorodihydrofluorescein Diacetate; **DCF:** 2′,7′-Dichlorofluorescein; **DMEM:** Dulbecco's Modified Eagle Medium; **DMSO:** Dimethyl Sulfoxide; **DNA:** Deoxyribonucleic Acid; **ED_{50}:** Effective Dose 50%; **EtBr:** Ethidium Bromide; **FBS:** Fetal Bovine Serum; **FITC:** Fluorescein Isothiocyanate; **HCT116:** Human Colorectal Cancer Cell Line; **IC_{50}:** Half-Maximal Inhibitory Concentration; **LMPA:** Low-Melting-Point Agarose; **MTT:** 3-(4,5-Dimethylthiazol-2-yl)-2,5-Diphenyl Tetrazolium Bromide; **NMPA:** Normal-Melting-Point Agarose; **OD:** Optical Density; **PBS:** Phosphate-Buffered Saline; **PDB:** Protein Data Bank; **PI:** Propidium Iodide; ROS**:** Reactive Oxygen Species; **SD:** Standard Deviation; **SN:** Secondary Necrotic; **VI:** Viable; **EA:** Early Apoptotic; **LA:** Late Apoptotic.

CONFLICT OF INTEREST

The authors declare that there is no conflict of interest.

ETHICAL STATEMENT

Not applicable, as this study used a commercially obtained cell line and did not involve human participants or animals.

AUTHORS CONTRIBUTION

Both authors have contributed equally to research, lab work and writing.

DATA AVAILABILITY

Available on reasonable request from authors.

SUMMARY

Colorectal cancer remains a major global health challenge, highlighting the need for effective and safer therapeutic agents. This study investigated the anticancer potential and apoptotic mechanism of conessine, a plant-derived steroidal alkaloid, in HCT116 human colorectal cancer cells. Conessine demonstrated dose-dependent cytotoxicity, with an IC_{50} of 76.949 µg/mL. Treatment significantly increased apoptotic cell death, as confirmed by Annexin V/PI flow cytometry and AO/EtBr dual staining, accompanied by chromatin condensation and nuclear fragmentation. The comet assay revealed substantial DNA damage, while increased intracellular ROS indicated oxidative stress as a potential upstream mechanism. Molecular docking further demonstrated favourable interactions of conessine with Bcl-2 and Bax. Overall, conessine shows promising anticancer activity through ROS-associated DNA damage and apoptosis.

REFERENCES

1. Fink H, Langselius O, Vignat J, Rumgay H, Rehm J, Martinez RX, *et al.* Global and regional cancer burden attributable to modifiable risk factors to inform prevention. Nature Medicine 2026;32(4):1306-15.
2. Siegel RL, Wagle NS, Star J, Kratzer TB, Smith RA, Jemal A. Colorectal cancer statistics, 2026. CA: A Cancer Journal for Clinicians 2026;76(2):e70067.
3. Debela DT, Muzazu SG, Heraro KD, Ndalama MT, Mesele BW, Haile DC, Kitui SK, Manyazewal T. New approaches and procedures for cancer treatment: Current perspectives. SAGE open medicine. 2021 Aug;9:20503121211034366.
4. Asma ST, Acaroz U, Imre K, Morar A, Shah SRA, Hussain SZ, *et al.* Natural products/bioactive compounds as a source of anticancer drugs. Cancers 2022;14(24):6203.
5. Khan AW, Farooq M, Haseeb M, Choi S. Role of plant-derived active constituents in cancer treatment and their mechanisms of action. Cells 2022;11(8):1326.
6. Dua VK, Verma G, Singh B, Rajan A, Bagai U, Agarwal DD, *et al.* Anti-malarial property of steroidal alkaloid conessine isolated from the bark of *Holarrhena antidysenterica*. Malaria journal 2013;12(1):194.
7. Guo D, Guo Y, Zhu C, Liao Y, Lin Z, Zhang H, Zhang W, Zou Z. Programmed cell death network in cancer drug resistance: a framework for therapeutic intervention. Drug Resistance Updates. 2026 Mar 5:101387.
8. Alshammari BO, Wadaan MA, Baabbad A, Mohany M, Damra E, Hozzein WN. Organic Extract of Streptomyces Induces Apoptosis, Anti-Proliferation and Cell-Cycle Arrest in Colon Cancer Cells: Caco-2 and HCT116 Cell Line as Surrogate Model. Indian Journal of Animal Research 2024;58(2):233-40.
9. Azqueta A, Muruzabal D, Boutet-Robinet E, Milic M, Dusinska M, Brunborg G, Møller P, Collins AR. Technical recommendations to perform the alkaline standard and enzyme-modified comet assay in human biomonitoring studies. Mutation Research/Genetic Toxicology and Environmental Mutagenesis. 2019 Jul 1;843:24-32.
10. Boyraz MÜ, Shekhany B, Süzergöz F. Cellular imaging analysis of MTT assay based on tetrazolium reduction. Harran Üniversitesi Tıp Fakültesi Dergisi 2021;18(1):95-9.
11. Alshehade SA, Almoustafa HA, Alshawsh MA, Chik Z. Flow cytometry-based quantitative analysis of cellular protein expression in apoptosis subpopulations: A protocol. Heliyon. 2024 Jul 15;10(13).
12. Collins A, Møller P, Gajski G, Vodenková S, Abdulwahed A, Anderson D, *et al.* Measuring DNA modifications with the comet assay: a compendium of protocols. Nature protocols 2023;18(3):929-89.
13. Diller DJ, Merz Jr KM. High throughput docking for library design and library prioritization. Proteins: Structure, Function, and Bioinformatics 2001;43(2):113-24.
14. Shoaib S, Ansari MA, Fatease AA, Safhi AY, Hani U, Jahan R, *et al.* Plant-derived bioactive compounds in the management of neurodegenerative disorders: challenges, future directions and molecular mechanisms involved in neuroprotection. Pharmaceutics 2023;15(3):749.
15. Majumder S, Panigrahi GK. Phytochemicals as modulators of autophagy and apoptosis: unveiling synergistic mechanisms in cancer therapy. Plant Sci. Today [Internet]. 2025;12(4). https://doi.org/10.14719/pst.8034
16. Fatma H, Jameel M, Siddique HR. An update on phytochemicals in redox homeostasis:"virtuous or evil" in cancer chemoprevention? Chemistry 2023;5(1):201-22.
17. Kaur K, Thomas S, Daggett M, TremL J. The Pro-Apoptotic Effects of Curcumin on HCT116 Colorectal Cancer Cells. Midwestern Journal of Undergraduate Sciences 2025;4(1):48-52.
18. Ratanabunyong S, Siriwaseree J, Wanaragthai P, Krobthong S, Yingchutrakul Y, Kuaprasert B, *et al.* Exploring the apoptotic effects of sericin on HCT116 cells through comprehensive nanostring transcriptomics and proteomics analysis. Scientific Reports 2024;14(1):2366.
19. Parhira S, Zhu G, Wangteeraprasert A, Sawong S, Suknoppakit P, Somran J, *et al.* Enhancement of apoptosis in HCT116 and HepG2 cells by *Coix lacryma-jobi var. lacryma-jobi* seed extract in combination with sorafenib. Chinese Herbal Medicines 2025;17(2):322-39.
20. Chen Y, Men L. Artemetin Inhibits Cell Growth and Activates Caspase-dependent Apoptotic Cell Death Colon Cancer HCT-116 Cells. Pharmacognosy Magazine 2025;21(4):1212-9.
21. Jiang N, Naz S, Ma Y, Ullah Q, Khan MZ, Wang J, *et al.* An overview of comet assay application for detecting DNA damage in aquatic animals. Agriculture 2023;13(3):623.
22. Alsubaie S, Merghani N, Abudawood M, Siddiqi NJ, Fatima S. Comparative Mechanistic Insights into Quercetin-Loaded Selenium Nanoparticles and Cisplatin in HCT116 Cells. ACS omega 2025;10(47):57123-36.
23. Mahmoud K, Mohammed A, Salem D, Ibrahim K, Shawky M, Osama M, *et al*. Cytotoxic, Genotoxic and pro-apoptotic effect of some medicinal plants on the expression of colon cancer-related genes (P53 & Bcl2) in the colorectal cell line and syngenic animal cancer model. Egyptian Journal of Chemistry 2022;65(11):761-77.
24. da Silva EL, Mesquita FP, de Farias Ramos IN, Rego CB, dos Santos Moreira C, Ferreira VF, da Rocha DR, de Oliveira Bahia M, Moreira-Nunes CA, de Souza CR, Burbano RM. Antitumoral effect of novel synthetic 8-hydroxy-2-((4-nitrophenyl) thio) naphthalene-1, 4-dione (CNN16) via ROS-mediated DNA damage, apoptosis and anti-migratory effect in colon cancer cell line. Toxicology and Applied Pharmacology. 2022 Dec 1;456:116256.
25. An X, Yu W, Liu J, Tang D, Yang L, Chen X. Oxidative cell death in cancer: mechanisms and therapeutic opportunities. Cell Death & Disease 2024;15(8):556.
26. Soumya T, Lakshmipriya T, Klika KD, Jayasree P, Manish Kumar P. Anticancer potential of rhizome extract and a labdane diterpenoid from *Curcuma mutabilis* plant endemic to Western Ghats of India. Scientific Reports 2021;11(1):552.
27. Radwan Z, Kassir R, Al Feghaly F, Zaiter R, Daher MA, Roufayel R, *et al.* Anticancer Activity of *Jania rubens* in HCT-116 Cells via EMT Suppression, TET Downregulation, and ROS-Mediated Cytotoxicity. Biomolecules 2025;15(10):1361.

28. Kaltsas A, Markou E, Kyrgiafini M-A, Zikopoulos A, Symeonidis EN, Dimitriadis F, *et al.* Oxidative-stress-mediated epigenetic dysregulation in spermatogenesis: implications for male infertility and offspring health. Genes 2025;16(1):93.
29. Parveen S, Ahtsham A, Kumar S, Gupta P, Ghous F, Banerjee M. Piperlongumine mediated apoptosis in cervical cancer cells beyond docking predictions. Toxicology Reports. 2025 Jun 1;14:102031.
30. Srinivas US, Tan BW, Vellayappan BA, Jeyasekharan AD. ROS and the DNA damage response in cancer. Redox biology. 2019 Jul 1;25:101084.
31. Wolf P, Schoeniger A, Edlich F. Pro-apoptotic complexes of BAX and BAK on the outer mitochondrial membrane. Biochimica et Biophysica Acta (BBA)-Molecular Cell Research 2022;1869(10):119317.
32. Srinivas US, Tan BW, Vellayappan BA, Jeyasekharan AD. ROS and the DNA damage response in cancer. Redox biology 2019;25:101084.
33. Mansour MA, El-Salamoni MA, Mostafa HN. Harnessing PUMA's lethal potential: BCL-2 family dynamics and novel strategies to combat cancer recurrence. Cancer Treatment and Research Communications. 2025 Jul 29:100975.
34. Putri GFT. Bax/Bcl-2 ratio as the golden marker of apoptosis: molecular mechanisms and regulatory pathways. International Journal of Cell and Biomedical Science 2025;4(10):309-17.

Cite this article: Makeen HA, Albratty M, Halawi MA. Conessine Induces Apoptosis Associated with Oxidative Stress and DNA Damage in HCT116 Colorectal Cancer Cells: An *in vitro* and *in silico* Study. Indian J of Pharmaceutical Education and Research. 10.5530/ijper.20270127.